Structural, electrical transport, and magnetic properties of Ni1−xZnxFe2O4

ARTICLE *in* JOURNAL OF MAGNETISM AND MAGNETIC MATERIALS · MAY 2007

Impact Factor: 1.97 · DOI: 10.1016/j.jmmm.2006.09.030

5 AUTHORS, INCLUDING:

A.K.M. Akther Hossain
Bangladesh University of Engineering and…
84 PUBLICATIONS **536** CITATIONS
SEE PROFILE

S. T. Mahmud
University of Alberta
13 PUBLICATIONS **172** CITATIONS
SEE PROFILE

Munetoshi Seki
The University of Tokyo
31 PUBLICATIONS **394** CITATIONS
SEE PROFILE

Hitoshi Tabata
The University of Tokyo
211 PUBLICATIONS **6,949** CITATIONS
SEE PROFILE

Available online at www.sciencedirect.com
ScienceDirect
Journal of Magnetism and Magnetic Materials 312 (2007) 210–219
Journal of magnetism and magnetic materials
www.elsevier.com/locate/jmmm

Structural, electrical transport, and magnetic properties of $Ni_{1-x}Zn_xFe_2O_4$

A.K.M. Akther Hossain[a,*], S.T. Mahmud[a], M. Seki[b], T. Kawai[b], H. Tabata[b]

[a]*Department of Physics, Bangladesh University of Engineering and Technology, Dhaka 1000, Bangladesh*
[b]*Institute of Scientific and Industrial Research, Osaka University 8-1 Mihogaoka, Ibaraki, Osaka 567-0047, Japan*

Received 21 July 2006; received in revised form 22 September 2006
Available online 27 October 2006

Abstract

Structural, electrical, and magnetic properties of $Ni_{1-x}Zn_xFe_2O_4$ ($x = 0.2$, 0.4) samples sintered at various temperatures have been investigated thoroughly. The bulk density of the $Ni_{0.8}Zn_{0.2}Fe_2O_4$ samples increases as the sintering temperature (T_s) increases from 1200 to 1300 °C and above 1300 °C the bulk density decreases slightly. The $Ni_{0.6}Zn_{0.4}Fe_2O_4$ samples show similar behavior of changes to that of $Ni_{0.8}Zn_{0.2}Fe_2O_4$ samples, except that the bulk density is found to be the highest at 1350 °C. The DC electrical resistivity, $\rho(T)$, decreases as the temperature increases indicating that the samples have semiconductor-like behavior. As the Zn content increases, the Curie temperature (T_c), resistivity, and the activation energy decrease while the magnetization, initial permeability, and the relative quality factor (Q) increases. A *Hopkinson* peak is obtained near T_c in the real part of the initial permeability vs. temperature curves. The ferrite with higher permeability has a relatively lower resonance frequency. The initial permeability and magnetization of the samples has been found to correlate with density, average grain sizes. Possible explanation for the observed structural, magnetic, and changes of resistivity behavior with various Zn content are discussed.

PACS: 75.50.Gg

Keywords: Saturation magnetization; Grain size; Curie temperature; Resistivity

1. Introduction

Polycrystalline spinel ferrites are widely used in many electronic devices. These are preferred because of their high permeability in the radio-frequency (RF) region, high electrical resistivity, mechanical hardness, chemical stability, and reasonable cost [1–4]. Ferrites are also useful to prevent and eliminate RF interference to audio systems. According to their structure, it has tetrahedral A site and octahedral B site in AB_2O_4 crystal structure. It shows various magnetic properties depending on the composition and cation distribution. Various cations can be placed in A and B sites to tune its magnetic properties [2–15]. The antiferromagnetic A−B superexchange interaction is the main cause of the cooperative behavior of magnetic dipole moments in the ferrites, which is observed in Ni–Zn ferrites below their Curie temperature [4]. Leung et al. [5] performed a low-temperature Mössbauer study of $Zn_xN_{1-x}Fe_2O_4$. They found that for $x \leqslant 0.5$ the resultant A and B site Fe-spin moments have a collinear arrangement, whereas for $x > 0.5$ a non-collinear arrangement of A and B site Fe-spin moments exist. An explanation based on the relative strength of the exchange constant J_{AB} and J_{BB} is given to account for this difference. Soft ferrite applications are based on their ability to transform AC signals of small amplitude into substantially large variations of magnetic flux. The response of any magnetic material in an applied magnetic field can be understood on the basis of magnetic domains and domain walls. The value of the (relative) initial permeability gives a good indication of how easily a given material can be magnetized, since $\mu_r = 1$ represents the free space. Large permeability, i.e., substan-

*Corresponding author. Tel.: +88 (0)2 966 5613; fax: +88 (0)2 861 3046.
E-mail address: akmhossain@phy.buet.ac.bd (A.K.M.A. Hossain).

0304-8853/$ - see front matter © 2006 Elsevier B.V. All rights reserved.
doi:10.1016/j.jmmm.2006.09.030

tially, large magnetization produced by small field, can only occur because of domain walls [4]. Rosales et al. [16] measured the permeability of $Zn_{1-x}Ni_xFe_2O_4$ with $0.3 \leqslant x \leqslant 0.4$. They show that the relaxation frequency and magnetocrystalline anisotropy constant is related by the equation: $f_x = f_{x0} + AK_1$, where f_{x0} and A are constants. Recently, colossal magnetoresistance (CMR) effect has been observed in $ZnFe_2O_4$ and Ni substituted $Zn_{1-x}Ni_xFe_2O_4$ [2]. In this paper, we report structural, electrical, and magnetic (both DC and AC) properties of $N_{1-x}Zn_xFe_2O_4$ ($x = 0.2$ and 0.4) prepared at various sintering temperatures. In view of the importance of high frequency devices, we have analyzed AC magnetic behavior of samples at high frequency (1 kHz–13 MHz). Possible explanation for the observed character of magnetization, resistivity, and initial permeability of the studied samples are discussed. These experiments are expected to provide information to understand physical properties of the Ni–Zn ferrites.

2. Experimental

Ferrite samples with chemical formula $Ni_{1-x}Zn_xFe_2O_4$ ($x = 0.2$ and 0.4) were prepared using the standard solid-state reaction technique. Powders of NiO (99.9%), ZnO (99.999%), and Fe_2O_3 (99.99%) were used as raw materials. Stoichiometric amounts of required powders were mixed thoroughly and then calcined at 1100 °C for 24 h. The calcined powders were then pressed uniaxially into disk shaped (about 10 mm diameter, 2–3 mm thickness) and toroid shaped (about 10 mm outer diameter, 5 mm inner diameter, and 3 mm thickness) samples. The samples were sintered at various temperatures (1200, 1250, 1300, 1350, and 1400 °C) in air for 5 h. The temperature ramp was 10 °C/min for both cooling and heating.

Microstructural properties were investigated with a high-resolution optical microscope. X-ray diffraction was carried out with an X-ray diffractometer with Cu-K_α radiation. The theoretical density, ρ_{th}, was calculated using the expression, $\rho_{th} = 8M/N_A a_0^3$, where N_A is the Avogadro's number, M is the molecular weight, and a_0 is the lattice constant. The porosity was calculated using the relation $\left[100(\rho_{th} - \rho_B)/\rho_{th}\right]\%$, where ρ_B is the bulk density measured by the formula: $\rho_B = M/V$. Average grain sizes (grain diameter) of the samples were determined from optical micrographs by linear intercept technique [17].

The DC electrical resistivity ρ of the Ni–Zn ferrite samples was measured by standard four-point probe and the van der Pauw technique [18,19]. The activation energy (E) was determined from the temperature dependence of resistivity. The magnetization measurements were performed on pieces of samples (approximate dimensions $2 \times 1 \times 1\,mm^3$) using a quantum design SQUID magnetometer.

The frequency characteristics of the Ni–Zn ferrite samples i.e. the initial permeability spectra were investigated in a field of about 12 mOe using an Agilent impedance analyzer (model no. 4192A). The complex permeability measurements on toroid shaped specimens have been carried out at room temperature on all the samples in the frequency range 1 kHz–13 MHz. The values of the measured parameters obtained as a function of frequency and the real part (μ') of the complex permeability have been calculated using the following relations: $\mu' = L_s/L_0$, where L_s is the self-inductance of the sample core and $L_0 = \mu_0 N^2 S/\pi\bar{d}$ is derived geometrically. Here L_0 is the inductance of the winding coil without the sample core, N is the number of turns of the coil ($N = 5$), S is the area of cross section, and $\bar{d}$ is the mean diameter of the sample. The relative quality factor (Q) was calculated from the relation: $Q = \mu_i'/\tan\delta$, where $\tan\delta$ is the loss factor. The temperature dependent initial permeability was measured at a constant frequency (100 kHz) of a sinusoidal wave. The Curie temperature (T_c) of the samples was determined from the temperature dependent initial permeability measurement.

3. Results and discussion

3.1. Structural properties

The X-ray diffraction (XRD) patterns for the samples $Ni_{1-x}Zn_xFe_2O_4$ with $x = 0.2$, 0.4 are shown in Fig. 1. Analysing the XRD patterns, we notice that the positions of the peaks comply with the reported values [2]. The XRD patterns of both compositions clearly indicate their single phase and formation of spinel structure. The lattice parameter for each peak of each sample was calculated by using the formula: $a = d\sqrt{h^2 + k^2 + l^2}$, where h, k, and l are the Miller indices of the crystal planes. To determine the exact lattice parameter for each sample, Nelson–Riley method was used. The Nelson–Riley function $F(\theta)$ is given as $F(\theta) = \frac{1}{2}\left[(\cos^2\theta/\sin\theta) + (\cos^2\theta/\theta)\right]$. The values of lattice constant a of all the peaks for a sample was plotted against $F(\theta)$ (not shown). Then using a least square fit method exact lattice parameter a_0 was determined. The

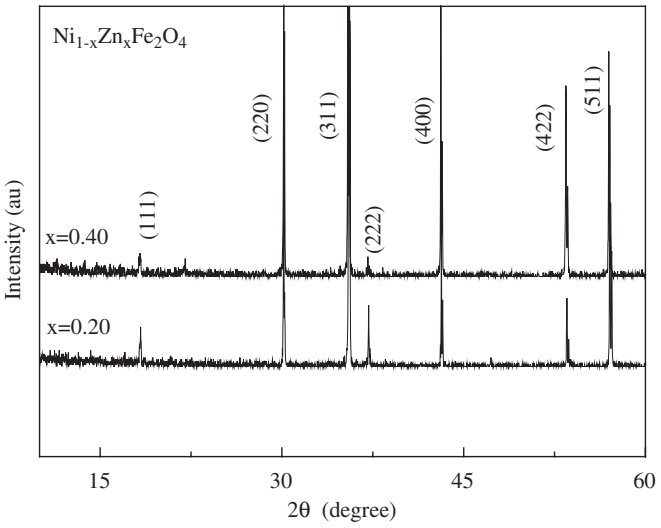

Fig. 1. The X-ray diffraction patterns for the samples $Ni_{1-x}Zn_xFe_2O_4$ with $x = 0.2$ and 0.4.

point where the least square fit straight line cut the y-axis (i.e. at $F(\theta) = 0$) is the actual lattice parameter of the sample. We observed that there is no noticeable variation of XRD pattern for a particular composition as a function of sintering temperatures.

The measured lattice parameter, density, porosity, and average grain size for various samples sintered at different temperatures are tabulated in Table 1. It can be seen from Table 1 that the lattice parameter increases with increasing Zn content for both the compositions. The increase in lattice parameter with increasing Zn content can be explained on the basis of the ionic radii. The radius of the Zn^{2+} (0.82 Å) is greater than that of the Ni^{2+} (0.78 Å) [2]. The density of the $Ni_{0.8}Zn_{0.2}Fe_2O_4$ samples increases as the sintering temperature increases from 1200 to 1300 °C and above 1300 °C the density decreases slightly. On the other hand, porosity (P) of the sample decreases as increasing sintering temperature up to 1300 °C, and above 1300 °C the porosity increases slightly. The $Ni_{0.6}Zn_{0.4}Fe_2O_4$ samples show similar behavior of changes to that of $Ni_{0.8}Zn_{0.2}Fe_2O_4$ samples except that density is found to be the highest at 1350 °C. It is known that the porosity of ceramic samples results from two sources, intragranular porosity and intergranular porosity [20]. Thus, the total porosity could be written as $P = P_{\text{intra}} + P_{\text{inter}}$. The intergranular porosity mainly depends on the grain size [20]. At higher sintering temperatures, the density decreases because the intragranular porosity increases resulting from discontinuous grain growth. This result agrees with that previously reported in case of MgCuZn ferrites [21].

The optical micrographs for $Ni_{0.8}Zn_{0.2}Fe_2O_4$ and $Ni_{0.6}Zn_{0.4}Fe_2O_4$ compositions sintered at various temperatures are shown in Fig. 2. It can be seen from Table 1 that the average grain size of the samples increases with an increase of Zn content and sintering temperature. The grain size has an important influence on the domain wall contributions in the magnetization process at low frequency. When the grain growth rate is very high, pores may be left behind by rapidly moving grain boundaries, resulting in pores that are trapped inside the grains. This intragranular porosity is practically impossible to eliminate, leading to poor magnetic, and mechanical properties. During the sintering process, the thermal energy generates a force that drives the grain boundaries to grow over pores, thereby decreasing the pore volume and densifying the material. The discontinuous growth of grain rises with temperature, hindering the migration of the pore to the grain boundary and hence, contributing toward the reduction of the bulk density.

3.2. DC electrical resistivity

The temperature dependence of DC electrical resistivity of Ni–Zn ferrite samples sintered at 1300 °C for 5 h is shown in Fig. 3. It is observed that the ferrite samples have semiconductor like behavior, where DC electrical resistivity (ρ) decreases on increasing the temperature. The $\rho(T)$ for both compositions follows $\rho(T) = \rho_0 \exp(E/k_B T)$, where E is the activation energy for electric conduction and ρ_0 is the pre-exponential constant. The DC resistivity, $\rho(T)$, also decreases as the Zn content increases. The values of $\rho(300\,\text{K})$ for studied samples are given in Table 2. It is reported that Zn ions prefer the occupation of tetrahedral (A) sites; Ni ions prefer the occupation of octahedral (B) sites while Fe ions partially occupy the A and B sites. The cation distribution of Ni−Zn ferrite is $(Zn_x^{2+}Fe_{1-x}^{3+})[Ni_{1-x}^{2+}Fe_{1+x}^{3+}]O_4^{2-}$, where the term within the square brackets indicates the octahedral (B) sites and the first term is tetrahedral (A) sites [3]. On increasing Zn content (at A sites), the Ni ion concentration (at B sites) will decrease. This will lead to the migration of some Fe^{3+} ions from A to B sites to substitute the reduction in Ni ion concentration at B sites. As a result, the number of Fe^{2+} and Fe^{3+} ions at B sites (which is responsible for electric conduction in ferrites) increases. Consequently, ρ decreases with increasing Zn content. Another reason for the decrease in ρ on increasing Zn ion substitution is that, zinc is less resistive than nickel [22]. The values of activation energy (E) in the ferrimagnetic region evaluated from the formula $E = 0.198 \times 10^{-3}(\delta(\log\rho)/\delta(1/T))$ (eV) is tabulated in Table 2. The present values of activation energy are in good agreement with the published results [22,23]. The small values for activation energy confirm the electronic character of the conduction process. The main conductivity mechan-

Table 1
Room temperature data for $Ni_{1-x}Zn_xFe_2O_4$ samples sintered at various temperatures with fixed dwell time 5 h in air

Sample composition	Sintering temperature (°C)	a_0 (Å)	ρ_{th} (g/cm^3)	ρ_B (g/cm^3)	P (%)	Grain size (μm)	f_r (MHz)
$Ni_{0.8}Zn_{0.2}Fe_2O_4$	1400			4.9693	7.1	13.1	5
	1350			4.9775	6.9	10.7	6
	1300	8.3638	5.35	4.9896	6.7	8.8	7
	1250			4.9306	7.8	7.2	12
	1200			4.5749	14.5	6.9	—
$Ni_{0.6}Zn_{0.4}Fe_2O_4$	1400			4.8632	9.4	24.7	3
	1350			4.9661	7.5	22.3	3
	1300	8.3705	5.37	4.9072	8.6	17.4	3
	1250			4.9010	8.72	11.7	4
	1200			4.8163	10.3	8.9	9

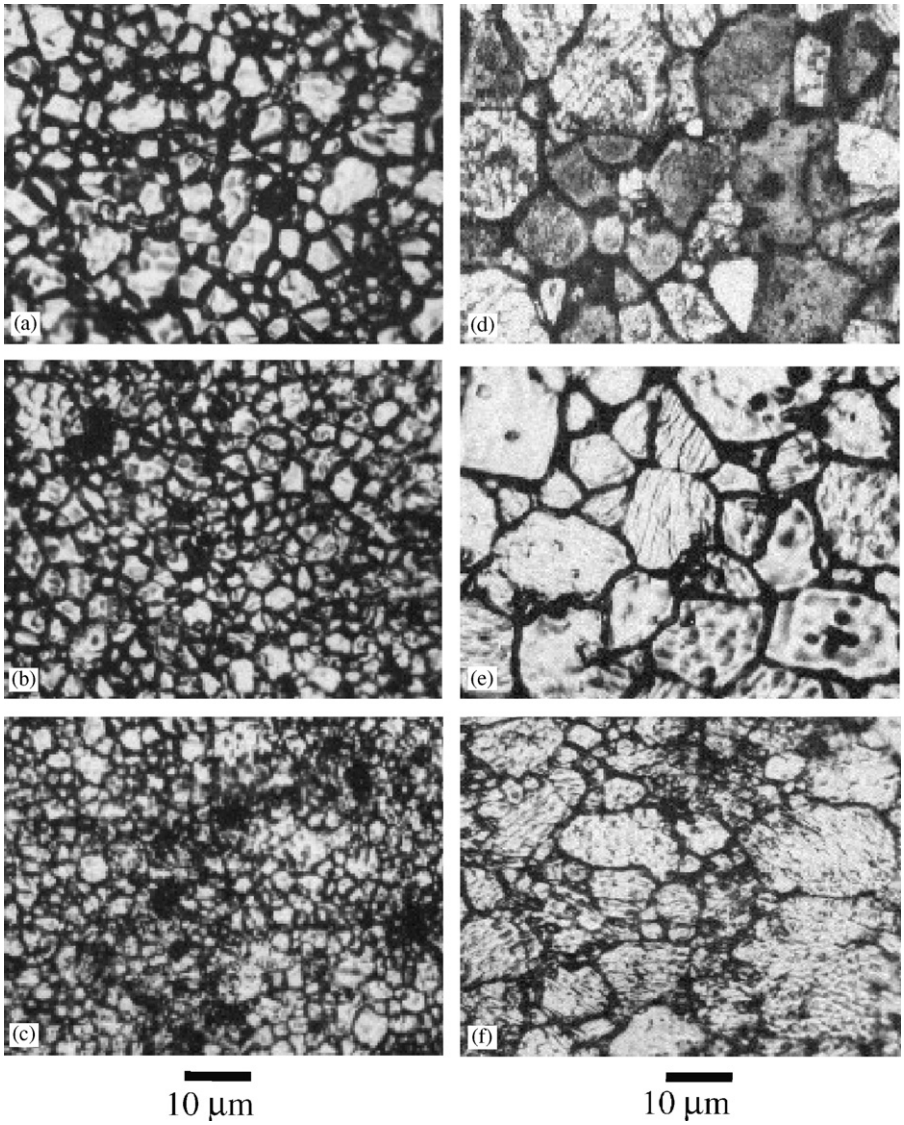

Fig. 2. The optical micrographs of $Ni_{0.8}Zn_{0.2}Fe_2O_4$ samples sintered at temperatures (a) 1400 °C, (b) 1350 °C, (c) 1300 °C in air; and micrographs of $Ni_{0.6}Zn_{0.4}Fe_2O_4$ samples sintered at temperatures, (d) 1400 °C, (e) 1350 °C, and (f) 1300 °C in air.

ism in Ni–Zn ferrites is attributed to electron hopping between Fe^{3+} and Fe^{2+} ions in octahedral sites. The activation energy of electric conduction was found to decrease with increasing the non-magnetic Zn content in the measured compositions. This is in good accordance with the conclusion that the lower activation energy is associated with the lower electrical resistivity, i.e., with higher conductivity.

The ρ for various $Ni_{1-x}Zn_xFe_2O_4$ samples sintered at 1300 °C is shown in Fig. 4. The ρ as a function of Zn content at various temperatures (200, 250, and 300 K) is shown in this figure. All samples show similar behavior at these temperatures. Variation of the ρ as a function of Zn content has two maxima, one is for $x = 0.20$ and other at $x = 0.60$. It was observed that at higher Zn concentration (>0.6) ρ decrease systematically, ρ also decreases for $0.2 < x < 0.5$.

3.3. Magnetic properties

3.3.1. Magnetization

The variation of magnetization, M, with the static applied magnetic field, H, (up to 5 T) for investigated samples at various temperatures (10, 150, 200, 250, and 300 K) are shown in Fig. 5. The magnetization increases with increasing the applied magnetic field, attains its saturation value for fields higher than 0.30 T. It is observed that the saturation magnetization (M_s) decreases with increasing temperature. The values of M_s for samples studied at 300 K are given in Table 2. The M–H loops of Ni–Zn ferrite samples measured at 10 K are shown in Fig. 6. It is observed that the values of coercive field (H_c) for both compositions are quite low ($H_c < 6$ Oe). This indicates that the studied samples are soft ferrites. It is clear that the saturation magnetization M_s increases with increasing Zn

content. This result is expected because it is known that for $Ni_{1-x}Zn_xFe_2O_4$ there is a collinear spin arrangement with x up to 0.5 [2,5]. The net magnetization for collinear spin arrangement at temperature T ($T \leqslant T_c$) could be expressed as $M(T) = M_B(T) - M_A(T)$, where M_A and M_B are the magnetic moments of A and B sites, respectively. The substitution of Zn (on the A site) will lead to increase the Fe^{3+} ions on the B site and consequently the magnetization of the B site will increase. At the same time, the magnetization of A site will decrease according to decrease in the Fe^{3+} ion on A site. Accordingly, the net magnetization will increase with increasing Zn content in the range of $x \leqslant 0.5$. Using the above-mentioned cation distribution of Ni–Zn ferrite and taking the values of the magnetic moment of Fe^{3+}, Zn^{2+}, and Ni^{2+} as 5, 0, and 2 μ_B, respectively, the total magnetic moment per formula unit at 0 K could be written as $m_{th}(\mu_B) = x(10-2)+2$, where μ_B is the Bohr magneton. The values of $m_{th}(\mu_B)$ for both compositions are given in Table 2. The variations of M_s with temperature for both compositions sintered at 1300 °C are shown in Fig. 7. It is observed that the M_s decreases rapidly with temperature for $Ni_{0.6}Zn_{0.4}Fe_2O_4$ than that of $Ni_{0.8}Zn_{0.2}Fe_2O_4$. Extrapolating $M_s(T)$ to low temperature ($T \to 0$) for higher fields (1 T) enables us to obtain the experimental magnetic moment per formula unit m_{expt} at 0 K in Bohr magneton. The values of $m_{expt}(\mu_B)$ are tabulated in Table 2. It is seen that the experimental values are in good agreement with the calculated results (m_{th}).

Fig. 8 shows the variation of magnetic moment per formula unit as a function of Zn content (x) in $Ni_{1-x}Zn_xFe_2O_4$. The m_{th} is supposed to increase as a function of Zn content as discussed above. However, the m_{expt}(10 K) and m_{expt}(300 K) is found to increase as a function of Zn content up to $x = 0.5$. Beyond $x = 0.5$, the m_{expt} decreases due to the non-collinear spin arrangements in the octahedral cations.

3.3.2. Initial permeability and Curie temperature

Fig. 9 shows the real part of initial permeability (μ'_i) spectra for $Ni_{0.8}Zn_{0.2}Fe_2O_4$ and $Ni_{0.6}Zn_{0.4}Fe_2O_4$ samples. The permeability value increases with increasing Zn content in $Ni_{1-x}Zn_xFe_2O_4$. The similar result is obtained for DC magnetization. The values of μ'_i for samples sintered at 1300 °C are tabulated in Table 2. In case of various $Ni_{0.8}Zn_{0.2}Fe_2O_4$ samples, μ'_i increases as the T_s increases up to 1300 °C and above 1300 °C, μ'_i decreases. The $Ni_{0.6}Zn_{0.4}Fe_2O_4$ samples show similar change of permeability to that of $Ni_{0.8}Zn_{0.2}Fe_2O_4$ samples except that μ'_i is found to be maximum at 1350 °C (optimum T_s).

As the T_s increases, the resonance frequency shifted from 12 to 5 MHz for $Ni_{0.8}Zn_{0.2}Fe_2O_4$ samples, and from 9 to 3 MHz for $Ni_{0.6}Zn_{0.4}Fe_2O_4$ samples. The μ'_i values for all

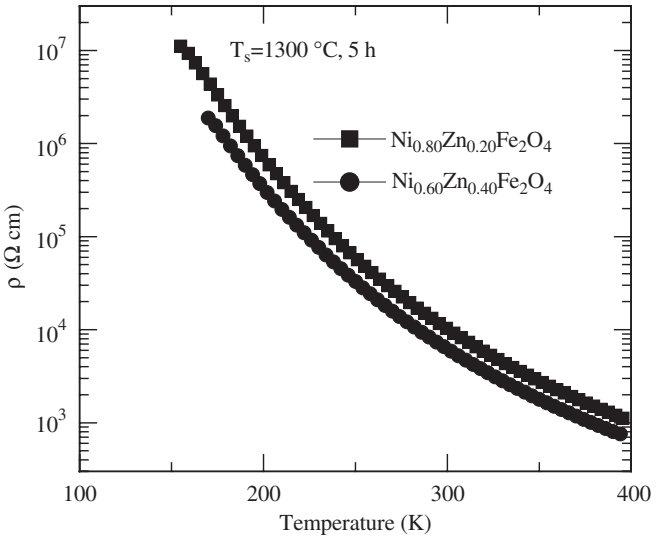

Fig. 3. The temperature dependence of the DC electrical resistivity for Ni–Zn ferrite samples sintered at 1300 °C for 5 h in air.

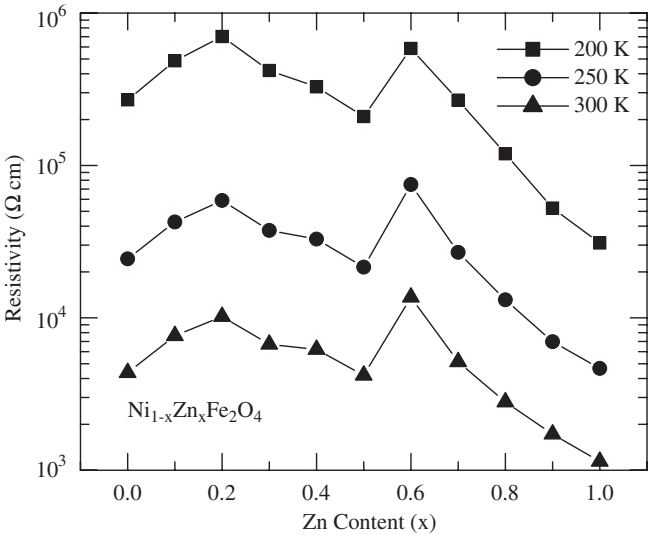

Fig. 4. Resistivity of $Ni_{1-x}Zn_xFe_2O_4$ samples as a function of Zn content at various temperatures. All samples were sintered at 1300 °C.

Table 2
The values of ρ (300 K), activation energy (E), M_s (300 K), m_{expt} (0 K), m_{th}(0 K), μ'_i, and Q at room temperature for Ni–Zn ferrite samples sintered at 1300 °C for 5 h in air

Sample composition	ρ (300 K) (Ω cm)	E (eV)	M_s (300 K) (emu/g)	m_{expt} (μ_B)	m_{th} (μ_B)	μ'_I (1 MHz)	Q (1 MHz)
$Ni_{0.8}Zn_{0.2}Fe_2O_4$	1.0×10^4	0.24	71	3.7	3.6	116	5.6×10^3
$Ni_{0.6}Zn_{0.4}Fe_2O_4$	6.2×10^3	0.22	79	5.0	5.2	274	3.1×10^3

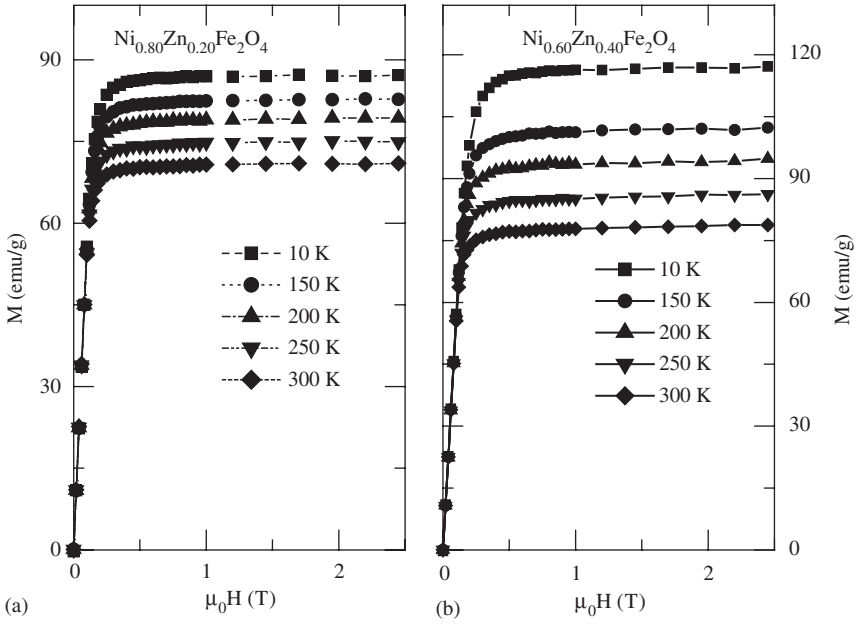

Fig. 5. The magnetization (M) versus the applied magnetic field (H) curves for (a) $Ni_{0.8}Zn_{0.2}Fe_2O_4$ and (b) $Ni_{0.6}Zn_{0.4}Fe_2O_4$ sample measured at 10, 150, 200, 250, and 300 K. Samples sintered at 1300 °C for 5 h in air.

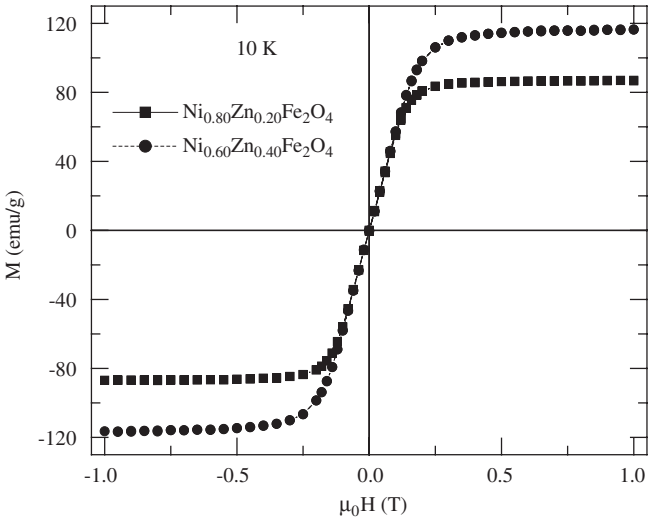

Fig. 6. The M–H loops of Ni–Zn ferrite samples measured at 10 K. Samples sintered at 1300 °C for 5 h in air.

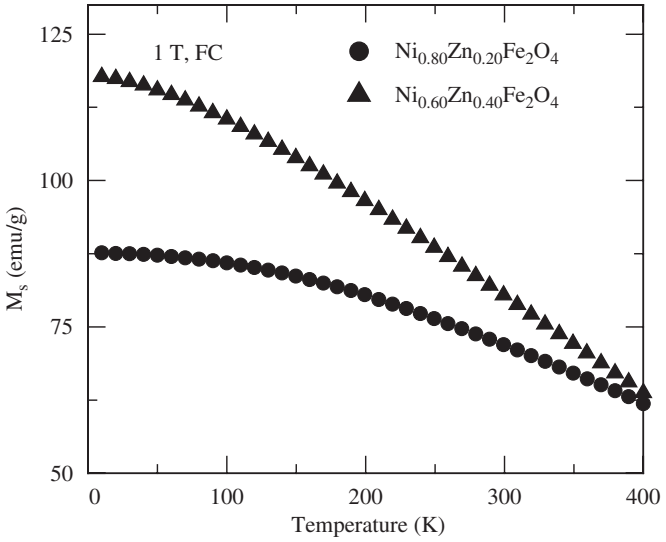

Fig. 7. The temperature dependence of Magnetization for Ni–Zn ferrite samples measured in a field of 1 T. Samples sintered at 1300 °C for 5 h in air.

samples are found independent of frequency below the resonance frequency. Above the resonance frequency μ'_i sharply decreases. The resonance frequencies (f_r) for all samples are tabulated in Table 1. The ferrite with higher permeability tends to have its permeability decreases at a relatively lower frequency.

It is well known that the permeability of polycrystalline ferrite is related to two different magnetizing mechanisms: spin rotation and domain wall motion [24,25], which can be described as follows:

$$\mu_i = 1 + \chi_w + \chi_{spin}, \quad (1)$$

where χ_w is the domain wall susceptibility; χ_{spin} is intrinsic rotational susceptibility. The χ_w and χ_{spin} may be written as: $\chi_w = 3\pi M_s^2 D/4\gamma$ and $\chi_{spin} = 2\pi M_s^2/K$, where M_s is the saturation magnetization, K the total anisotropy, D the average grain diameter, and γ the domain wall energy. Thus, the domain wall motion is affected by the grain size and enhanced with the increase of grain size. The initial permeability is therefore a function of grain size and magnetization. In our microstructural study, we have seen that Zn promotes sintering and hence increases the grain size. Larger grains tend to consist of a greater number of domain walls. As the number of walls increases with the grain sizes, the contribution of wall movement to magnetization increases. We also see that the magnetiza-

tion increases with increasing Zn content. Therefore, permeability increases with the increase of Zn content.

The study of microstructures reveals that the average grain sizes increases with increasing T_s. Thus for a large grain, permeability should increase as it varies proportionally with grain diameter. Thus one can expect higher μ'_i for the sample sintered at higher T_s. However, we have observed that for both the compositions μ'_i is found to be highest at optimum T_s (depending on sample composition) as shown in Fig. 10. If the sintering temperature is higher than that of the optimum T_s, μ'_i decreases. It is possible that the samples sintered at higher sintering temperatures ($\geqslant$optimum T_s) may increase the number of pores within the grains, which results in a decrease in permeability. Similar behavior was observed by Guillaud [26] in Mn–Zn ferrites. It is clear that, if pores can be suppressed or located at the grain boundaries, the permeability may increase with grain size. The relationship between grain size and permeability would generally be linear only if the grain growth is normal, that is, if all the grains grow pretty much at the same time and same rate. The pores at the grain boundaries is less damaging to the permeability, because it causes less hindrance to domain wall motion than pores within grains.

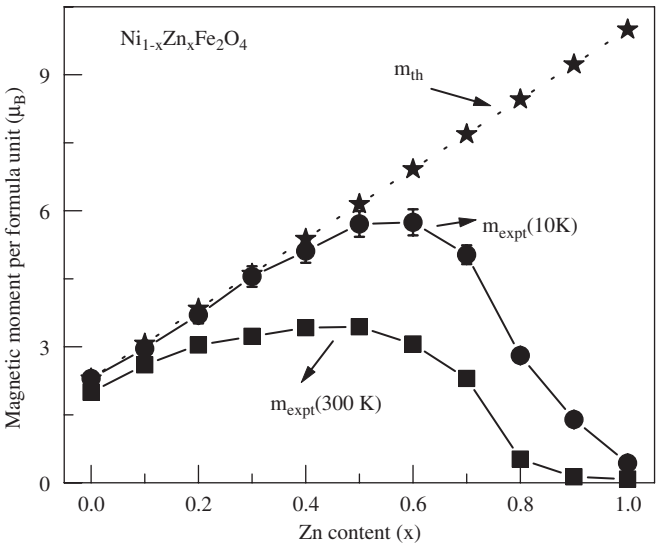

Fig. 8. Theoretically predicted magnetic moment and experimental magnetic moment per formula unit for various $Ni_{1-x}Zn_xFe_2O_4$ samples sintered at 1300 °C.

Both compositions obviously show relaxation resonance; with the real part μ'_i decreases drastically at high frequency above 3 MHz (depending on compositions and T_s). If the applied alternating field is weak, at high frequencies, the domain wall will oscillate back, and forth through a small distance about the mean position. The differential equation for oscillating boundaries can be written as $m(d^2x/dt^2) + \beta(dx/dt) + \alpha x = 2M_sH(t)$, where m is the effective wall mass, β the damping factor, α the restoring constant, x the wall displacement and $H(t)$ the driving force [4,27]. The first term on the left-hand side represents the wall inertia; the second term is the damping opposing the propagation velocity, and the third term is associated with wall pinning to defects, expressed as a restoring force. It is also observed that the higher the permeability of the material, the lower the frequency of the onset of ferrimagnetic resonance. This really confirms with Snoek's limit $f_r\mu'_i = \text{Constant}$ [28], where f_r is the resonance frequency for domain wall motion, above which μ'_i decreases. This means that there is an effective limit to the product of resonance frequency and permeability, so that high frequency and high permeability are mutually incompatible.

For polycrystalline material it has been shown [16,29] that the resonance frequency can be related to the anisotropy constant by $f_r = \text{constant} \times K_1$; i.e., the resonance frequency decreases with the decrease of anisotropy constant. The f_r variation can be attributed to variation of K_1, which mainly depends on the

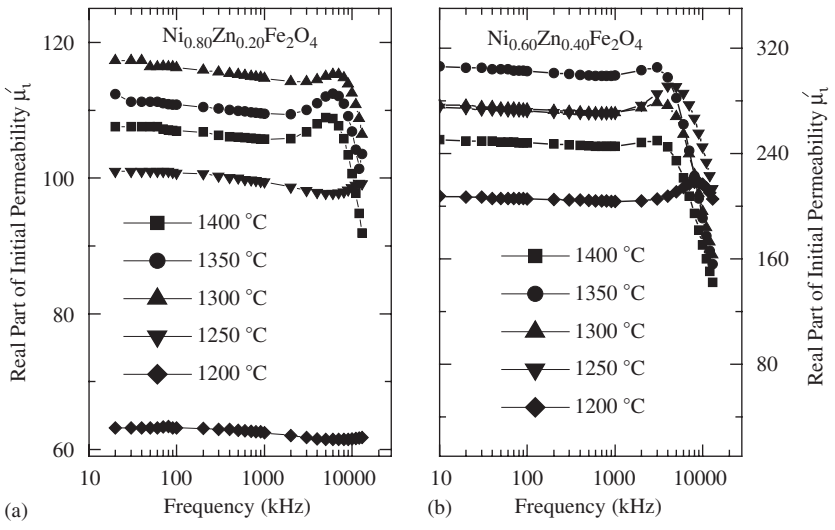

Fig. 9. The frequency dependence of initial permeability for (a) $Ni_{0.8}Zn_{0.2}Fe_2O_4$ and (b) $Ni_{0.6}Zn_{0.4}Fe_2O_4$ samples sintered at temperatures 1200, 1250, 1300, 1350, and 1400 °C for 5 h in air.

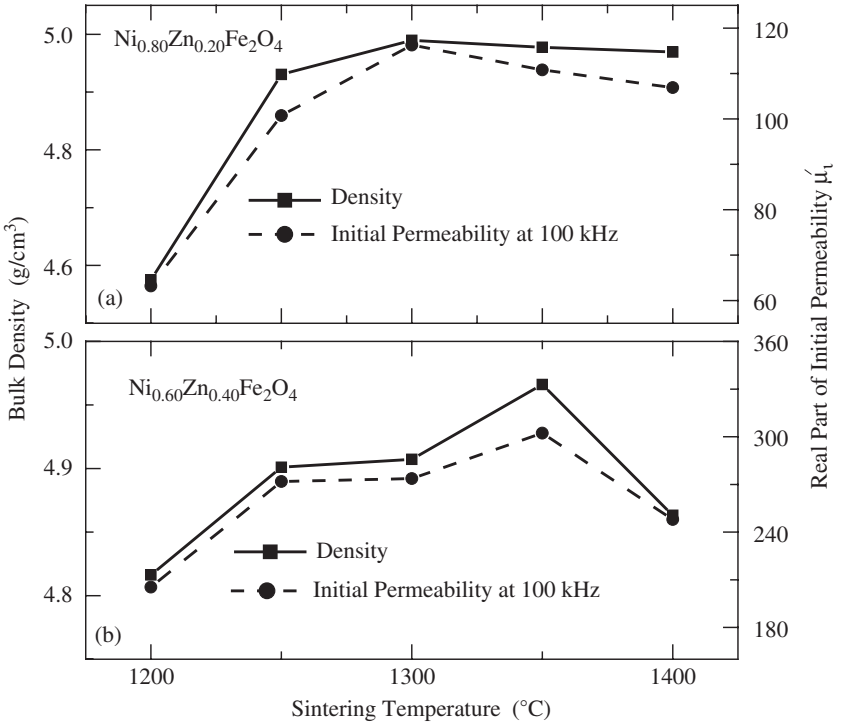

Fig. 10. Effect of sintering temperature (T_s) on the densification and μ_i' for (a) $Ni_{0.8}Zn_{0.2}Fe_2O_4$ and (b) $Ni_{0.6}Zn_{0.4}Fe_2O_4$ samples.

microstructure and composition. In permeability spectrum, it is seen that the resonance frequency decrease with the increase of Zn content. This is because Zn in these compositions not only increases the magnetic moment, but also lowers anisotropy [3]. On the other hand, the permeability increases with a decrease of K_1, as we know from the relation $\mu_i \approx M_S^2/K_1^{1/2}$ [4,29]. The high permeability values at low frequencies show the dominant role played by wall motion.

The variations of relative quality factor (or Q factor) with frequency for both composition sintered at various temperatures are shown in Fig. 11. For practical applications, the quality factor is often used as a measure of performance. It is observed that the sample sintered at 1200 °C has highest Q value for $Ni_{0.8}Zn_{0.2}Fe_2O_4$, while 1250 °C for $Ni_{0.6}Zn_{0.4}Fe_2O_4$. The highest Q value at 1250 °C for $Ni_{0.6}Zn_{0.4}Fe_2O_4$, while 1200 °C for $Ni_{0.8}Zn_{0.2}Fe_2O_4$ is probably due to the growth of lesser imperfection and defects in them compared to those in the samples sintered at higher T_s, which enhance frequency of hopping electrons between Fe^{2+} and Fe^{3+}. Smaller grain size is competent for larger Q values. For this reason, some grades of Ni–Zn ferrites are deliberately sintered at low temperature. The values of Q for the samples sintered at 1300 °C are given in Table 2. The highest Q value for $Ni_{0.6}Zn_{0.4}Fe_2O_4$ is found to be 2.1×10^4 at 1250 °C sintering temperature.

The temperature dependent initial permeability for both compositions is shown in Fig. 12. It is observed that the permeability falls sharply when the magnetic state of the ferrite samples changes from ferrimagnetic to paramagnetic. The vertical drop of the permeability at the Curie point indicates the degree of homogeneity in the sample composition [30,31]. The present samples have showed an excellent degree of homogeneity. The values of T_c as compared with published results are listed in Table 3. The present values of T_c's are in good agreement with the published results. The variations among the present results and the published results could be related to the variation in the preparation condition.

It is observed that the T_c is lower when Zn content is higher. This is expected because of the inclusion of higher concentration of non-magnetic Zn in the materials. This is in harmony with the theoretical and experimental findings. It is also observed that the T_c slightly increases with increasing sintering temperature for both compositions.

The decrease of T_c with an increasing Zn content may be explained by a modification of the A–B exchange interaction strength due to the change of the Fe^{3+} distribution between A and B sites. The decrease of the T_c is due to the weakening of the A–B interaction. This could be attributed to the increase in distance between the moments of A and B sites, which is confirmed by the increase in the lattice parameter with increasing Zn content. The larger distances between moments in samples $Ni_{0.6}Zn_{0.4}Fe_2O_4$ leads to decrease the A–B interaction relative to that of $Ni_{0.8}Zn_{0.2}Fe_2O_4$ samples and consequently the T_c decreases.

It is well known that anisotropy constants vary considerably with temperature. In most cases, anisotropy decreases steeply from a high value (at lower temperature), slowly decreases down to zero at T_c [4]. It is observed that the μ'_i increases with temperature to a maximum value just

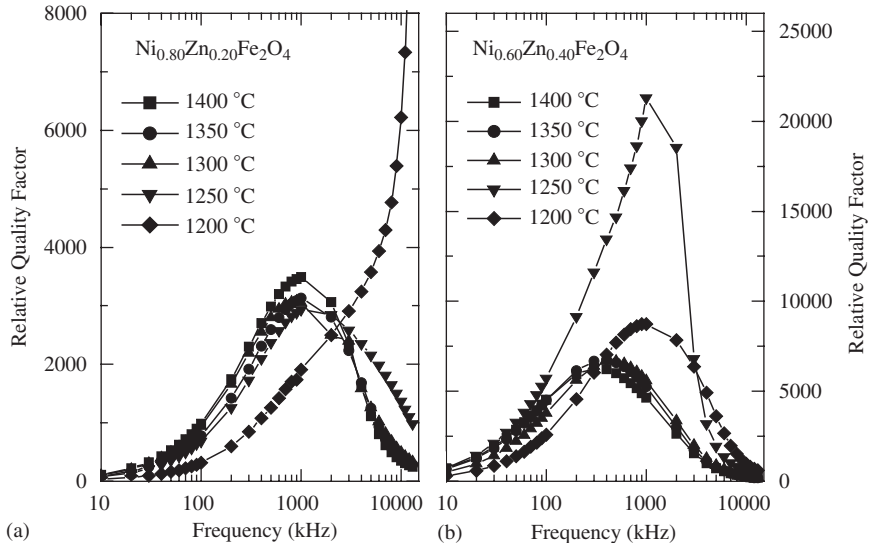

Fig. 11. The variation of Q factor with frequency for (a) $Ni_{0.8}Zn_{0.2}Fe_2O_4$ and (b) $Ni_{0.6}Zn_{0.4}Fe_2O_4$ samples sintered at temperatures 1200, 1250, 1300, 1350, and 1400 °C for 5 h in air.

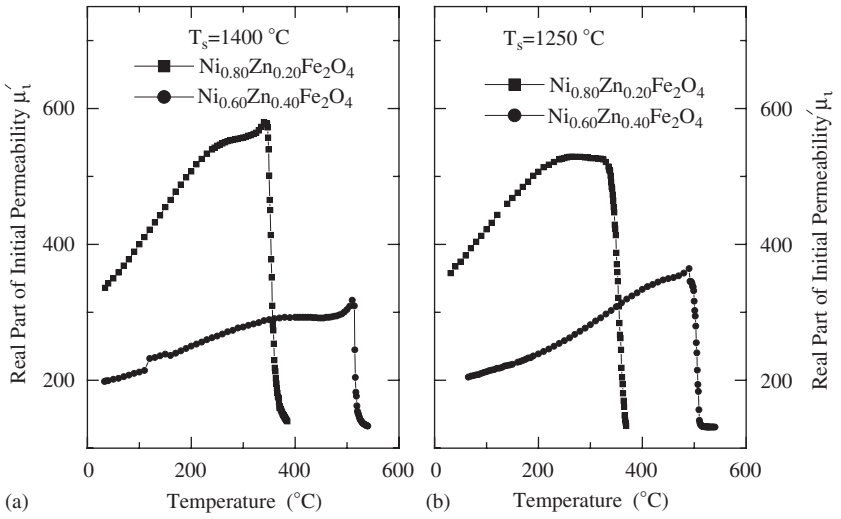

Fig. 12. The temperature dependence of the initial permeability for Ni–Zn ferrite samples sintered at (a) 1400 °C and (b) 1250 °C for 5 h in air.

Table 3
The values of Curie temperature, T_c, compared with the published results

Sample composition	T_s (°C)	Present T_c (°C)	Published results [Ref.] T_c (°C)
$Ni_{0.8}Zn_{0.2}Fe_2O_4$	1400	516 ± 1	512 [32], 480 [33], 476 [34]
	1250	506 ± 1	
$Ni_{0.6}Zn_{0.4}Fe_2O_4$	1400	353 ± 1	350 [33], 352 [35], 357 [22]
	1250	350 ± 1	

below the T_c. This occurs, because the crystal anisotropy normally decreases with increasing temperature [36]. The initial permeability varies as $\mu_i \approx M_s^2/K_1^{1/2}$ [4,29]. Since anisotropy decreases faster than magnetization on heating, the initial permeability, expectantly increases with temperature, tends to infinity just below the T_c and then drops for the paramagnetic phase. The peak near T_c is known as the '*Hopkinson*' peak [4].

4. Conclusions

The bulk density of the samples increases with sintering temperature up to optimum T_s (depending on composition). The DC electrical resistivity, $\rho(T)$, decreases as temperature increases indicating that the samples are semiconductors. As the Zn content increases, the electrical resistivity, activation energy and the T_c decreases while the magnetization, initial permeability and the relative quality factor increases. The initial permeability proportionally changes with bulk density. The permeability drops off at f_r because of the occurrence of ferrimagnetic resonance. This factor limits the frequency at which a magnetic material can be useful. The ferrite with higher permeability tends to

have its permeability decreases at a relatively lower frequency. This is because of the fact that the addition of Zn content increases the permeability, but lowers the resonance frequency by lowering the anisotropy. The requirements of high permeability and high working frequency lead to a compromise, since for a given composition, an increase in grain size leads simultaneously to an increase in permeability and decrease in resonance frequency. The choice of the basic composition also represents a compromise, since both resonance frequency and permeability are related to crystalline anisotropy.

References

[1] R. Peelamedu, C. Grimes, D. Agrawal, R. Roy, J. Mater. Res. 18 (2003) 2292.
[2] A.K.M. Akther Hossain, M. Seki, T. Kawai, H. Tabata, J. Appl. Phys. 96 (2004) 1273.
[3] A. Goldman, Handbook of Modern Ferromagnetic Materials, Kulwer Academic Publishers, Boston, USA, 1999.
[4] R. Valenzuela, Magnetic Ceramics, Cambridge University Press, Cambridge, 1994.
[5] L.K. Leung, B.J. Evans, A.H. Morrish, Phys. Rev. B 8 (1973) 29.
[6] W. Schiessl, W. Potzel, H. Karzel, M. Steiner, G.M. Kalvius, Phys. Rev. B 53 (1996) 9143.
[7] J.M. Hasting, L.M. Corliss, Phys. Rev. 102 (1956) 1460.
[8] J.M. Hasting, L.M. Corliss, Rev. Mod. Phys. 15 (1953) 114.
[9] Y.G. Chukalkin, A.E. Teplykh, Phys. Solid State 40 (8) (1998) 1364.
[10] M.A. Ahmed, N. Okasa, L. Salah, J. Magn. Magn. Mater. 264 (2003) 241.
[11] N. Rezlescu, E. Rezlescu, C. Pasnicu, M.L. Craus, J. Phys. Condens. Matter 6 (1994) 5707.
[12] O.F. Caltun, L. Spinu, A. Stancu, J. Optoelectron. Adv. Mater. 4 (2) (2002) 337.
[13] A. Gonochar, V. Andreev, L. Letyuk, A. Shishkanov, V. Maiorov, J. Magn. Magn. Mater. 254 (2003) 544.
[14] S.T. Mahmud, A.K.M. Akther Hossain, A.K.M. Abdul Hakim, M. Seki, T. Kawai, H. Tabata, J. Magn. Magn. Mater. 305 (2006) 269.
[15] E. Rezlescu, L. Sachelarie, P.D. Popa, N. Rezlescu, IEEE Trans. Magn. 36 (2000) 3962.
[16] M.I. Rosales, E. Amano, M.P. Cuautle, R. Valenzuela, Mater. Sci. Eng. B 49 (1997) 221.
[17] M.I. Mendelson, J. Am. Ceram. Soc. 52 (8) (1969) 443.
[18] L.J. van der Pauw, Philips Res. Rep. 13 (1958) 1.
[19] L.J. van der Pauw, Philips Tech. Rev. 20 (1958) 220.
[20] A.A. Sattar, H.M. El-Sayed, K.M. El-Shokrofy, M.M. El-Tabey, J. Appl. Sci. 5 (1) (2005) 162.
[21] S.R. Murthy, Bull. Mater. Sci. 24 (4) (2001) 379.
[22] M. El-Shabasy, J. Magn. Magn. Mater. 172 (1997) 188.
[23] A.M. Abdeen, J. Magn. Magn. Mater. 185 (1998) 199.
[24] Y. Mi, H. Jun, J. Zhejiang Univ. Sci. 6B (6) (2005) 580.
[25] T. Tsutaoka, M. Ueshima, T. Tokunaga, T. Nakamura, K. Hatakeyama, J. Appl. Phys. 78 (6) (1995) 3983.
[26] C. Guillaud, Proc. IEE 104B (1957) 165.
[27] F. Brailsford, Physical Principles of Magnetism, D. Van Nostrand Company Ltd., London, 1966.
[28] J.L. Snoek, Physica 14 (1948) 207.
[29] S. Chikazumi, Physics of Magnetism, John Wiley & Sons, Inc., New York, 1966.
[30] E. Cedillo, J. Ocampo, V. Rivera, R. Valenzuela, J. Phys. F: Sci. Instrument 13 (1980) 383.
[31] R. Valenzuela, J. Mater. Sci. 15 (1980) 3137.
[32] G. Ranga Mohan, D. Ravinder, A.V. Ramana Reddy, B.S. Boyanov, Mater. Lett. 40 (1999) 39.
[33] C. Koops, Phys. Rev. 83 (1953) 121.
[34] A. Verma, T.C. Goel, R.G. Mendiratta, P. Kishan, J. Magn. Magn. Mater. 208 (2000) 13.
[35] P. Reddy, K. Pratap, T. Rao, Cryst. Res. Technol. 22 (1987) 977.
[36] B.D. Cullity, Introduction to Magnetic Materials, Addison-Wisley Publishing Company Inc., California, 1972.